Electronic Supplementary Material (ESI) for Journal of Materials Chemistry A.

Film morphology evolution during solvent vapor annealing of highly efficient small molecule donor/acceptor blends

Sebastian Engmann, Hyun Wook Ro, Andrew Herzing, Chad R. Snyder, Lee J. Richter,
Materials Science and Engineering Division, National Institute of Standards and Technology, Gaithersburg, MD 20899, USA

Paul B. Geraghty, David J. Jones
School of Chemistry, Bio21 Institute, The University of Melbourne, 30 Flemington Road, Parkville, Victoria 3010, Australia

Supporting Information

GISAXS Background Correction

Small angle scattering data was obtained near the sample horizon ($q_z \approx 0$) as shown in Figure S 1. The extracted 1D profiles were weighted by the square of the scattering vector in order to obtain so called Kratky Plots. In order to account for a background offset of the data, a constant offset in *I(q)* for *q*-values > 0.1 Å^{-1} was assumed and subtracted from the data.

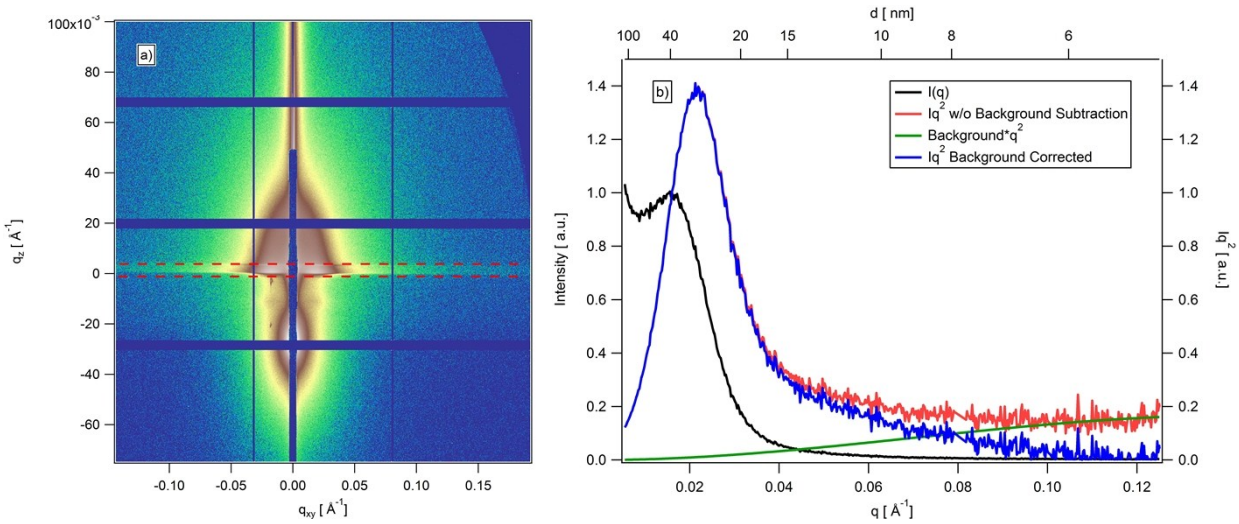

Figure S 1 - GISAXS Detector Image (a) and extracted 1D line profile near the sample horizon (b). Also shown in b) are the q²-weighted scattering intensity before and after background subtraction. The data corresponds to a dry BTR/PC$_{71}$BM BHJS after 30 s SVA with THF.

Comparison AFM vs TEM vs GISAXS

We have performed 2D FFTs of the AFM and TEM images of the as-cast, and post deposition annealed BTR BHJs presented in the mansucript. The following figure shows a comparison of the radially averaged and q^2 weighted FFT data and the GISAXS data. The GISAXS and TEM are in

good agreement, justifying the GISAXS analysis. The AFM clearly captures a radically coarser length scale.

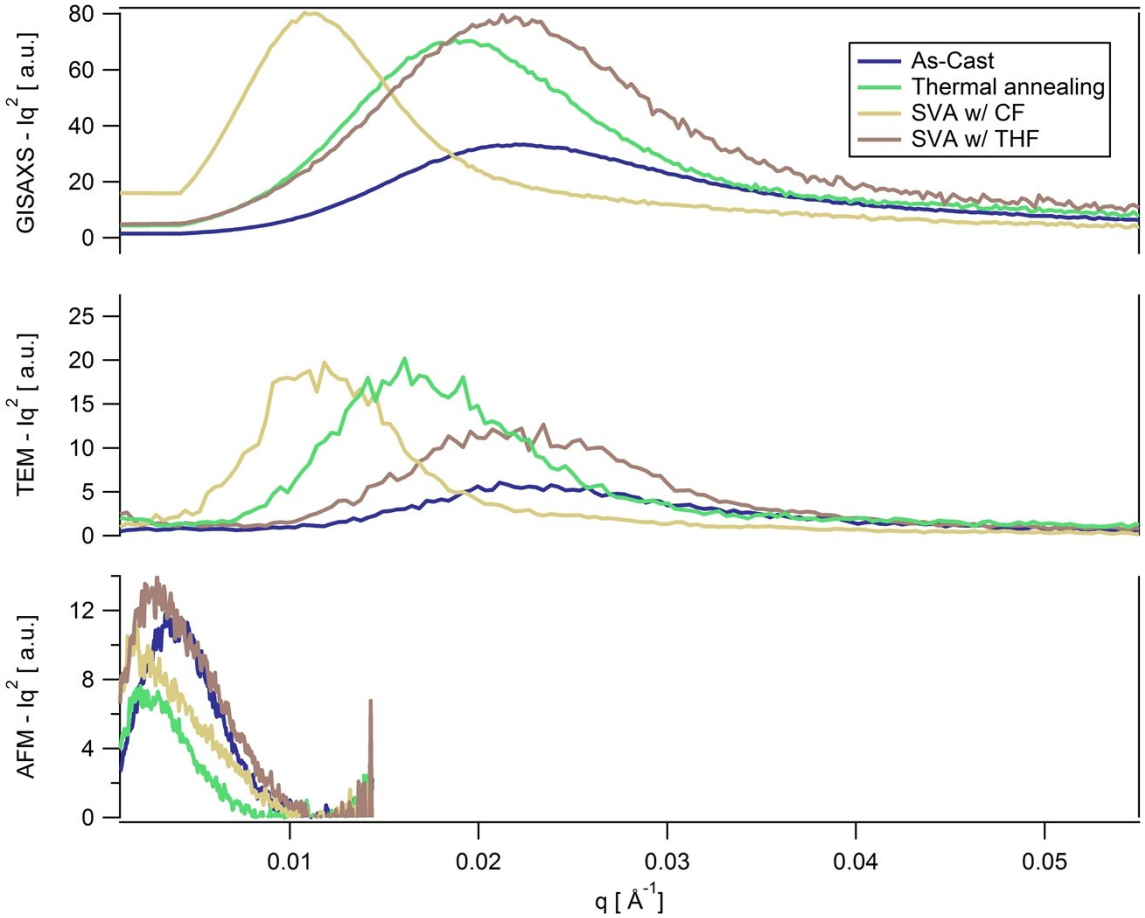

Figure S 2 – Radially averaged FFT data of the AFM & TEM images (bottom & middle) in comparison to the GISAXS data (Kratky plots, top).

White Light Interferometry / In-Situ Reflection

During all in situ experiments normal incidence reflection data was recorded in order to allow the extraction of film thickness and swelling during the SVA and thermal annealing experiments. The reflection spectra were corrected for parasitic reflection of the SVA window. Single reflection spectra were fitted using a transfer matrix algorithm in which the sample was represented by Si/PEDOT:PSS(20 nm)/active layer. The thickness of the PEDOT:PSS layer was determined prior the deposition of the BTR/$PC_{71}BM$ active layer and held constant (we neglect any swelling of this layer during SVA as PEDOT:PSS exhibits large polarity and is neither soluble in THF nor CF). The active layer was modeled using an effective medium approach (Bruggeman EMA) consisting of a higher and lower ordered BTR fraction, $PC_{71}BM$, and solvent. The refractive indices of BTR and $PC_{71}BM$ have been determined by spectroscopic ellipsometry prior to the study. The solvent refractive index was determined from transmission measurements and described in the transparent

region by a Cauchy dependence. During the fit the volume ratio of BTR to $PC_{71}BM$ was fixed to the nominal concentration of the prepared solution.

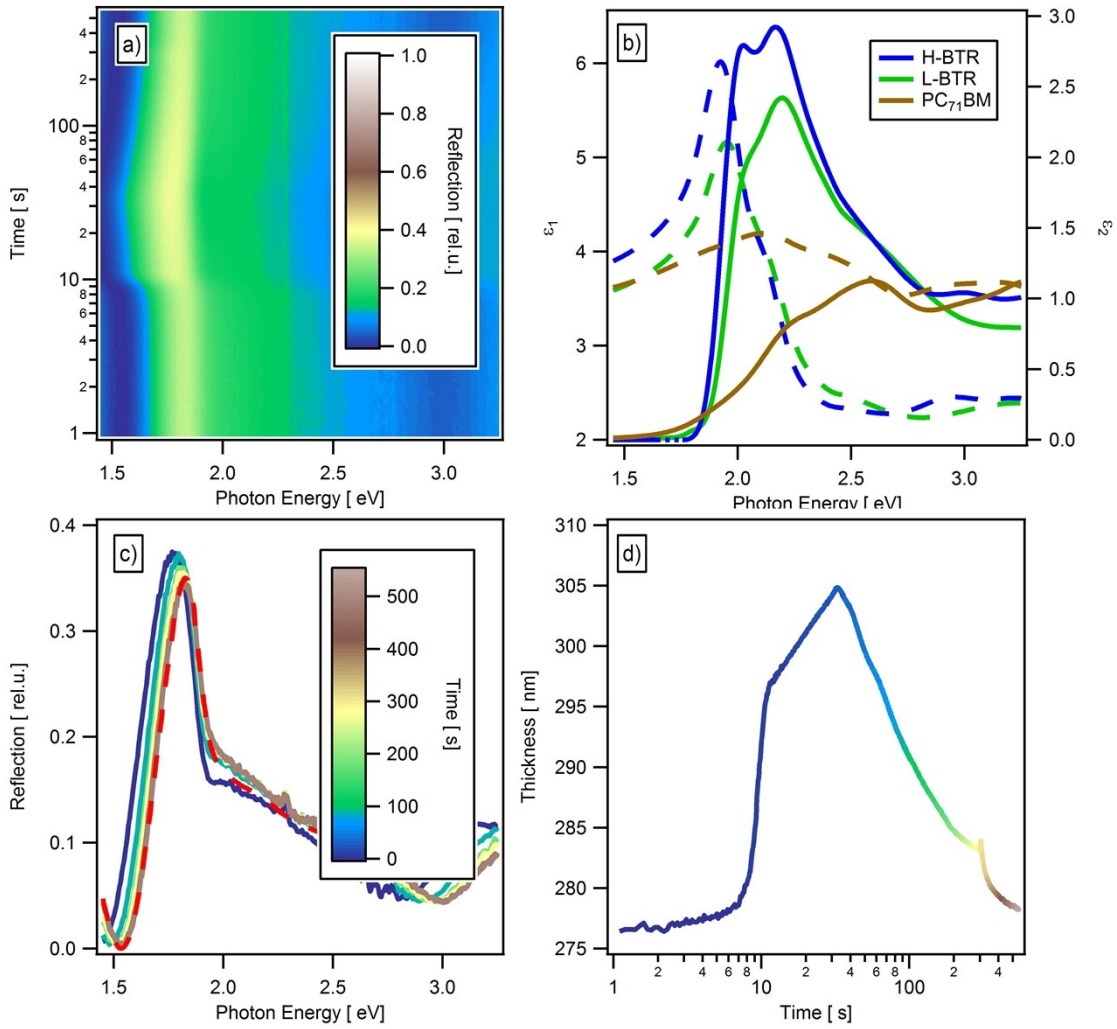

Figure S 3 – a) False Color representation of the in-situ normal incidence reflection data which was acquired simultaneously to the GIXD measurements of a BTR/$PC_{71}BM$ BHJ during 30 s SVA with THF. b)Real (broken lines) and imaginary part (solid lines) of the complex dielectric function of the used active layer materials. c) Selected reflection spectra for times between 0 and 500 s, showing the best fit of the reflection after 500 s. d) The film thickness shown in (d) was extracted from the fit of the reflection data.

BTR – $PC_{71}BM$ Bilayer Experiments

In order to investigate the ability of $PC_{71}BM$ to interdiffuse into amorphous BTR regions, we conducted bilayer stability experiments. Samples consisting of initially pure layers of the donor BTR and acceptor $PC_{71}BM$ have been thermally treated and the swelling of one of the layers by the other one was investigated using spectroscopic ellipsometry. For this purpose pristine BTR films were blade coated from a 30 mg/mL CF:CB solution on top of silicon wafers with natural oxide. The coating was performed inside a nitrogen filled glove box at a stage temperature of 45 °C, with blade velocity of 40 mm/s and blade-to-sample gap of 300 µm. Onto these films a thin $PC_{71}BM$ capping layer was transferred from a temporary substrate using a PDMS elastomer stamp.[1-3]

Release of the $PC_{71}BM$ layer from the temporary substrate (Si with natural oxide) was facilitated by soaking in deionized water. The samples were then annealed at 110 °C and 150 °C under inert atmosphere for 5 min. The post anneal distribution of $PC_{71}BM$ across the sample thickness was determined via spectroscopic ellipsometry measurements and optical modelling. The optical model consisted of 3 layers, each represented by an effective medium (Bruggeman EMA) consisting of $PC_{71}BM$ and BTR, on top of a silicon substrate. During the modelling, the film thickness and $PC_{71}BM$ volume fraction were fitted. The complex dielectric function (DF) of $PC_{71}BM$ was determined prior to the study and held constant throughout the fit procedure. The DF of BTR was determined on pristine films prior to the study and used as initial conditions. The DFs were determined using Woollam's B-Spline material layer, which is comparable to a classic wavelength-by-wavelength determination of the DF. However, instead of fitting each wavelength independently, the spectral range is divided into a smaller number of sub-sections / nodes. Between nodes the DF is interpolated using a spline dependence. The DF is forced to fulfill Kramers-Kronig consistence and positive imaginary part of the dielectric function. During the bilayer fits this DF was allowed to vary slightly to account for the observable absorption changes (red shift and evolution of vibronic features). The obtained results for the $PC_{71}BM$ distribution are summarized in Table S 1 as well as Figure S 4. Shown are the distribution of $PC_{71}BM$ throughout the film thickness of the bilayer stack for the as-prepared sample and after 5 min thermal annealing at 110 °C and 150 °C, as well as the film thickness of each of the 3 assumed layers.

	Thickness [nm]			Volume fraction $PC_{71}BM$ / EMA [vol.-%]			Equivalent Thickness [nm]	
	Bottom	Intermix	Top	Bottom	Interm.	Top	BTR	$PC_{71}BM$
As-Prepared	91 ± 7	3 ± 3	57 ± 5	0	22 ± 100	100	93	58
TA 5 min @ 110°C	66 ± 4	22 ± 3	50 ± 2	2 ± 5	50 ± 10	100 ± 1	76	62
TA 5 min @ 150°C	32 ± 2	50 ± 22	32 ±2	32 ± 12	50 ± 12	6 ± 18	77	37

Table S 1 – Summary of the Results obtained from the determination of the $PC_{71}BM$ distribution from spectroscopic ellipsometry.

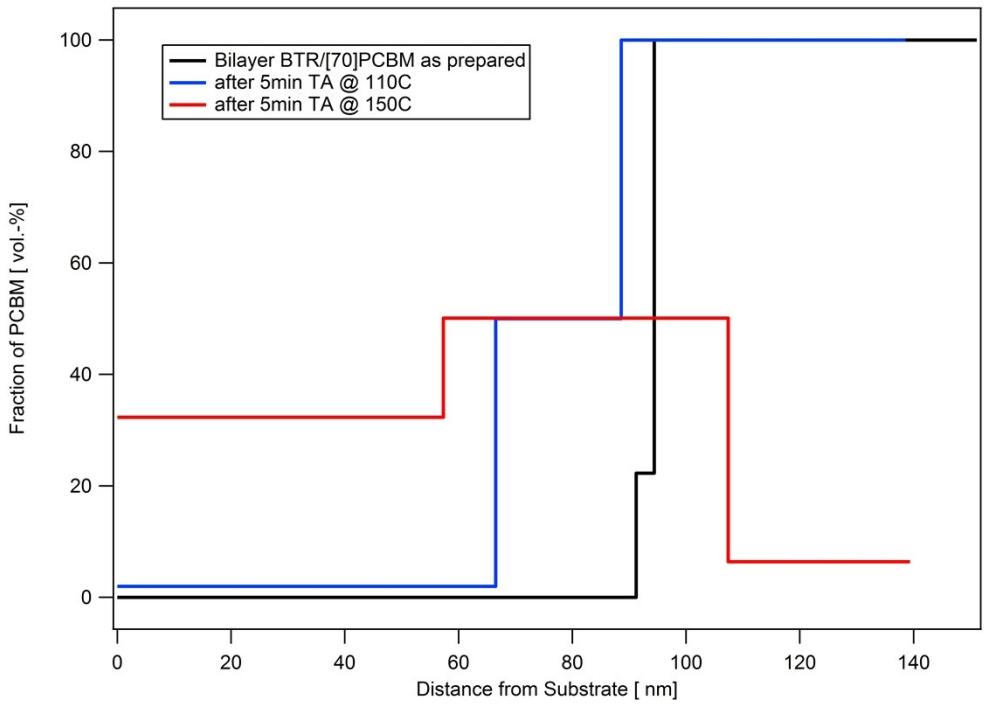

Figure S 4 – Distribution of the $PC_{71}BM$ volume fraction in an as-prepared BTR/$PC_{71}BM$ bilayer (black), after 5 min thermal annealing at 110 °C (blue) and after 5 +min annealing at 150 °C (red).

In case of the 110 °C thermal annealing the $PC_{71}BM$ distribution corresponds closely to that of the as-prepared film, indicating slow interdiffusion or low miscibility of the two initial layers into each other. Upon annealing at 150 °C the $PC_{71}BM$ distribution becomes more homogenous across the film thickness. Note that the uncertainty in the 150 °C is increased compared to the other two cases, due to film coarsening.

GIXD

The observed strong diffraction at about q = 0.343 is close to the (001), (010) and (01-1) features of the reported BTR single crystal structure. The powder diffraction pattern calculated by Mercury [4] based on the reported c*if-file* is shown in Figure S 5d. The strongest observable diffraction line in the powder diffraction corresponds to the (01-1) and its equivalent diffraction planes. Shown in Figure S 6 are the 3 respective orientations of the molecule with respect to the said diffraction plane. Both (010) and (01-1) correspond to nominally "edge-on" structure surfaces with solubility side chains facing the air and substrate interfaces.

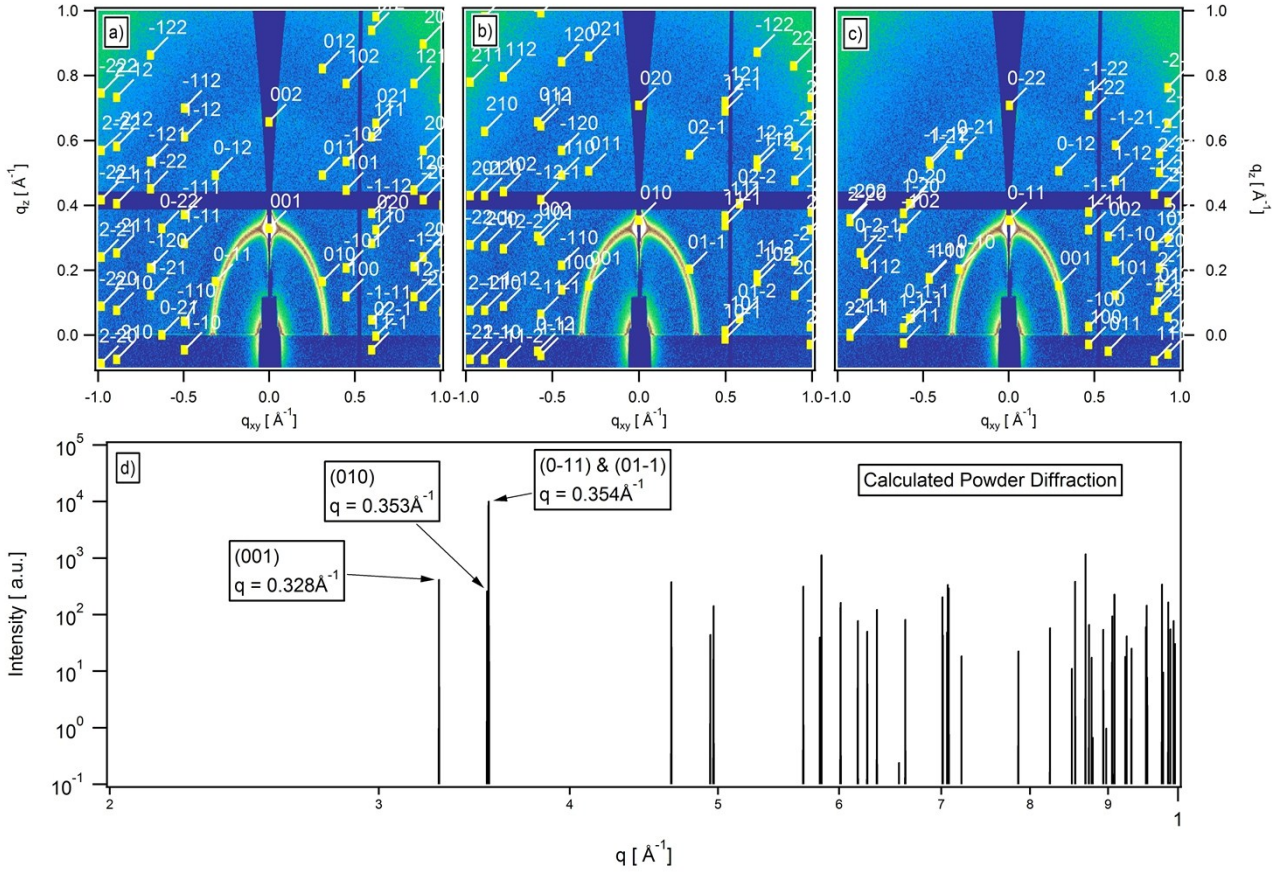

Figure S 5 – (a-c) Calculated position of diffraction peaks based on the BTR single crystal unit cell for 3 different crystal orientations. (d) Calculated powder diffractogram of BTR.

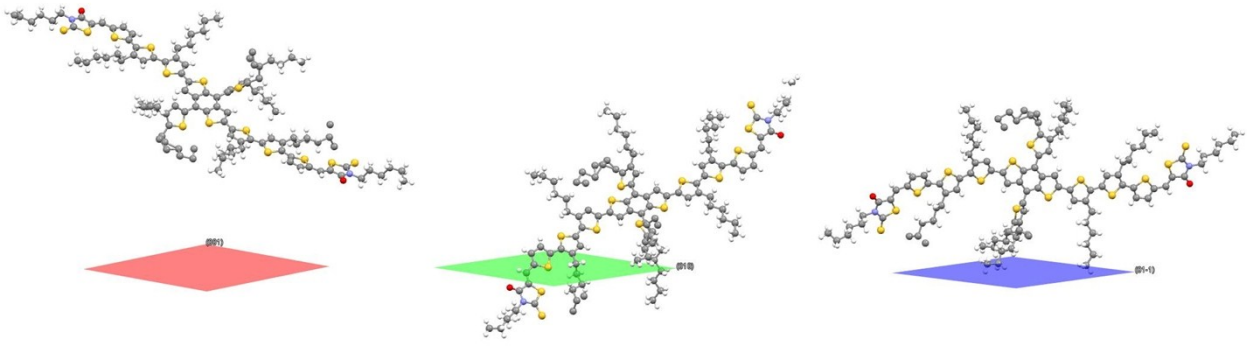

Figure S 6 – Diffraction planes (01-1), (010) and (01-1) for BTR's triclinic unit cell (left to right).

Estimation of Flory Interaction Parameter via Melting Point Depression

Differential Scanning Calorimetry (DSC) samples were prepared from BTR:PCBM solutions 25 mg/mL total mass in chloroform. Solutions of varying donor: acceptor ratio were prepared by mixing appropriate volumes of a pristine BTR and pristine PCBM stock solution. 100 µL of the mixed solution where dispensed under in inert atmosphere into low mass foil DSC pans designed for HyperDSC measurements and dried at 45°C. (Only one sample per loading was prepared, so the values derived should only be considered estimates.) Samples were measured with a PerkinElmer DSC8500 equipped with a liquid nitrogen chiller under a dry helium purge. Temperature and enthalpy calibrations were performed with indium and lead standards in the same low mass foil pans at the same heating rate as the samples. All samples were heated to 310 °C at 50 °C/min, held for 0.2 min, cooled at 50 °C/min to -40 °C, held for 2 min, and then heated to 310 °C again at 50 °C/min. Second heats are shown in Figure S 7. The data have been corrected for baseline curvature and artifacts due to mechanical instabilities in the pans at elevated temperatures (strong spikes in the heat flow data) the data shown are limited to the BTR melting range. No evidence of PCBM crystallization or melting was observed for the compositions studied. The melting traces were fit to three peaks, which have been attributed in order of increasing temperature to (1) a solid-solid crystal transition, (2) crystal melting to a liquid crystalline (LC) phase, and (3) LC isotropization (clearing). [5]

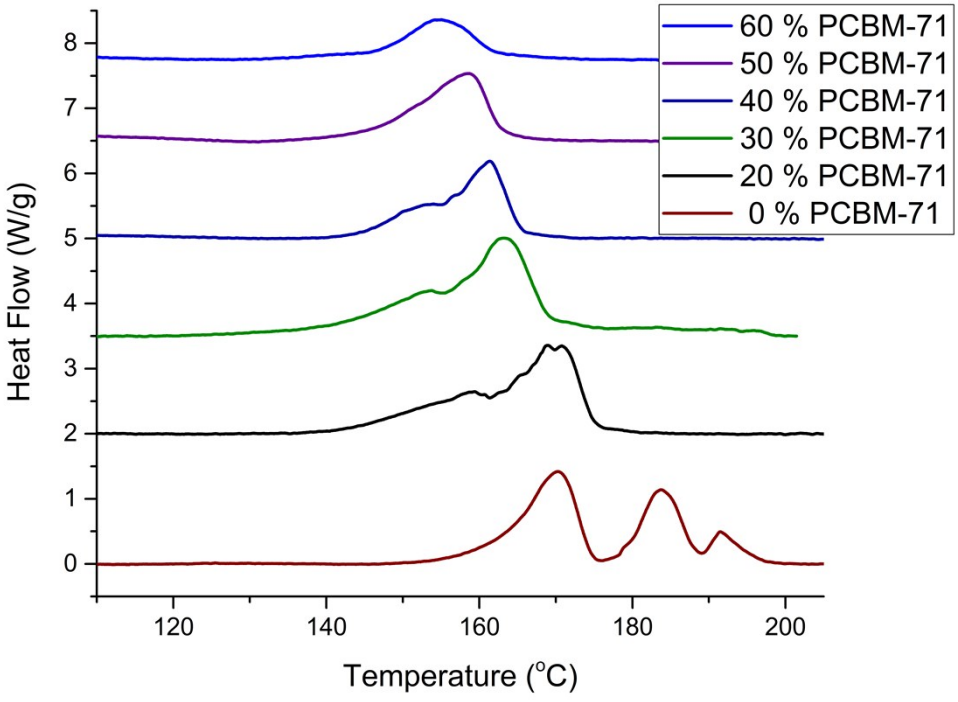

Figure S 7 – Typical DSC melting traces (endotherm direction is up) for BTR containing varying mass fractions of PCBM-71, as indicated in the legend. Traces have been corrected for baseline curvature.

The values for the crystalline melting peak temperature, derived from peak fitting, are plotted in Figure S 8. The melting point data were fit to Flory's melting point depression equation:[6]

$$\frac{1}{T_m} - \frac{1}{T_m^{\,0}} = \frac{R}{\Delta H_u}\left(\frac{v_u}{v_1}\right)\left[\varphi_1 - \chi\varphi_1^{\,2}\right]$$

where T_m is the observed melting temperature, T_m^0 is the equilibrium melting temperature (183.7±0.1) °C and ΔH_u is the enthalpy of fusion (12.7±0.1) kJ/mol both taken from the peak fit of the second heat of the neat BTR sample, R is the gas constant, v_u is the molar volume of the BTR, v_1 is the molar volume of the PCBM-71, ϕ_1 is the volume fraction of the PCBM, and χ is the Flory interaction parameter. The parameters that were allowed to float were v_u/v_1 and χ. The mass fraction (m_i) was converted to volume fraction ϕ_i for use in the equation via:

$$\varphi_1 = \frac{m_1}{(1-m_1)\left(\frac{\rho_1}{\rho_2}\right) + m_1}$$

where ρ_1 is the PCBM-71 density (1.58 g/cm^3) [3] and ρ_2 is the BTR density taken from the reported c*if-file* as 1.217 g/cm^3. The result of the fits were v_u/v_1=0.79±0.02 and χ=0.86±0.03. The value of v_u/v_1 is a factor of ≈3 less than the predicted value of 2.52 derived from the molar volumes of the two components, which is likely due to the fact that one is spherical and the other more planar suggesting different packing than would be indicated solely from the molar volumes.

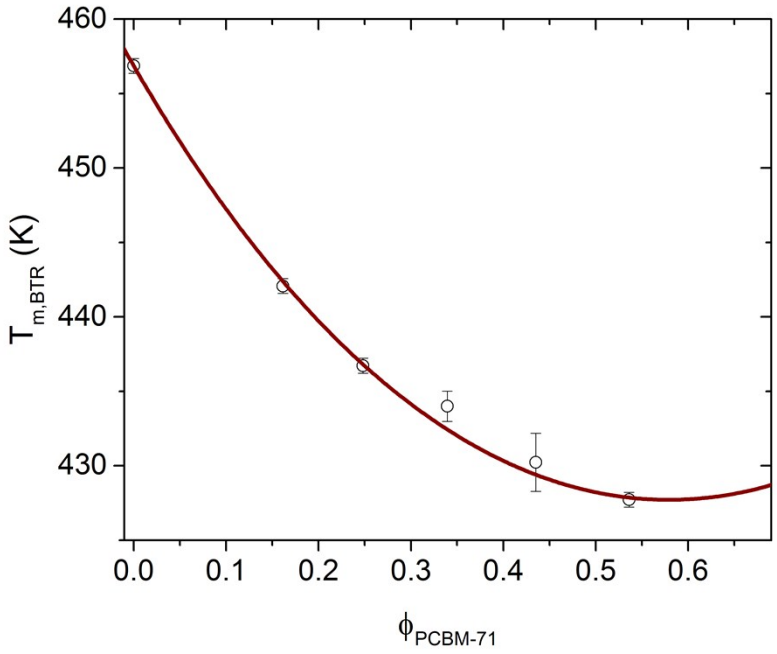

Figure S8 – Crystalline melting temperature of BTR as a function of volume fraction of $PC_{71}BM$. The line is a fit to Flory's melting point depression equation (see text).

Some final notes should be made related to the DSC measurements for possible future examination. On first heat of both the neat BTR powder and the drop cast pure BTR sample, there were four endotherms present rather than the three observed during the second heat. It is possible that this is the signature of an additional solid-solid transition. The lowest temperature endotherm is the one that appears to disappear in subsequent heating traces. Additionally, all three of the endotherms on second heat are shifted from (1 to 3) °C lower than their first heat values. The origin of the shift at this point remains unclear, it is doubtful that it is a contact issue as the drop cast sample had excellent contact with the foil pan. While degradation is a possible source for the shift, the degradation would have to be consistent across the loading series since a fit that excludes the 0 % $PC_{71}BM$ sample still extrapolates to the same T_m^0.

Bibliography

[1] H. W. Ro, B. Akgun, B. T. O'Connor, M. Hammond, R. J. Kline, C. R. Snyder*, et al.*, "Poly(3-hexylthiophene) and [6,6]-Phenyl-C61-butyric Acid Methyl Ester Mixing in Organic Solar Cells," *Macromolecules,* vol. 45, pp. 6587-6599, 2012/08/28 2012.

[2] O. Awartani, B. I. Lemanski, H. W. Ro, L. J. Richter, D. M. DeLongchamp, and B. T. O'Connor, "Correlating Stiffness, Ductility, and Morphology of Polymer:Fullerene Films for Solar Cell Applications," *Advanced Energy Materials,* vol. 3, pp. 399-406, 2013.

[3] D. Leman, M. A. Kelly, S. Ness, S. Engmann, A. Herzing, C. Snyder*, et al.*, "In Situ Characterization of Polymer–Fullerene Bilayer Stability," *Macromolecules,* vol. 48, pp. 383-392, 2015/01/27 2015.

[4] "Mercury," 3.5.1 ed: Cambridge Crystallographic Data Centre, 2015.

[5] K. Sun, Z. Xiao, S. Lu, W. Zajaczkowski, W. Pisula, E. Hanssen*, et al.*, "A molecular nematic liquid crystalline material for high-performance organic photovoltaics," *Nat Commun,* vol. 6, 01/14/online 2015.

[6] P. J. Flory, *Principles of Polymer Chemistry*: Ithaca, NewYork, Cornell University Press, 1953.